Annalen der Physik

annalen der physik
www.ann-phys.org

PERSPECTIVE OPEN ACCESS

Why Compressed Hydrides Are Near-Room-Temperature Superconductors

Warren E. Pickett

Department of Physics and Astronomy, University of California Davis, Davis, CA 95616, USA

Correspondence: Warren E. Pickett (wepickett@ucdavis.edu)

Received: 7 August 2025 | **Revised:** 6 October 2025 | **Accepted:** 30 October 2025

Keywords: atomic contributions | electron-phonon coupling | Eliashberg theory | hydride superconductivity | pressure effects

ABSTRACT

This Perspective provides a partial response to the titular statement since, as will be explained, the "why" – hydrogen atom scattering of Fermi surface electrons – is not yet understood. A pathway for achieving a more complete understanding is presented. This perspective addresses more specifically the question *why hydrogen, why so high* T_c, whose understanding remains limited. Based on as yet unapplied developments in simplifying aspects of metal hydride materials and separating out the effects of atomic displacements giving the atom-electron scattering, it is proposed that there is a straightforward path toward a deeper understanding of "metallic hydrogen superconductivity".

1 | Introduction

The 2014-2015 discovery by Emerets' group [1–3] of superconductivity (SC) up to T_c = 203 K in SH_3 in the 160–200 GPa range ignited a new era in SC research, and especially on understanding its microscopic origin and working toward even higher T_c SCs. Remarkably, this compound had been predicted (independently and published earlier) in 2014 by Duan et al. [4] using standard density functional theory (DFT) and Eliashberg formalism, to be a 200 K superconductor in the same pressure range. The following year saw extension of the calculations and explanation of the origins of very high T_c by several groups [5–12].

This breakthrough was followed by the prediction and discovery of LaH_{10} (T_c = 250–260 K around 200 GPa) [13–16] and soon after YH_9 (243 K at 200 GPa [17–19]) both also predicted before being confirmed by experimentalists, solidifying their origin as conventional, but now astounding, superconductors. The theory seems very robust, although H related corrections (anharmonicity, nonlinear coupling) may be necessary for accurate predictions. Half a dozen or more compressed metal hydrides with T_c above 100 K have been discovered since, displaying similarities and some differences.

These metal hydrides are phonon-paired superconductors, clear initially from the prediction of the first three hydrides, then dramatically supported by the exceptionally large H isotope effect [2] in SH_3. After decades of development of the formal theory and then implementation into computational packages, the current state of prediction of new superconductors is on firm grounds [20].

In spite of development and application of high-throughput searches (which necessarily require computational simplifications) of binary and ternary hydrides with several predictions of new and possibly better examples, experimental discovery of new examples has slowed. Quite possibly this limited success is partially due to some lack of crucial insight into the origin of high T_c, rather than or in addition to the now common approach of (i) considering the full phase diagram, (ii) selecting by some criteria the best suspects and checking for stability, then (iii) calculation of the Eliashberg spectral function α^2F and thereby T_c, insight that could provide focus to the search for better superconductors. This numerically taxing approach is being addressed by various groups, often using machine learning methods based on a sample dataset, with modest success so far. This paper presents the argument that there is one missing piece of the hydride puzzle

that should provide human insight and provide some focus for computational searches.

The organization of this Perspective is as follows. Section 2 introduces the specific terminology needed for this paper, noting the difference of the elemental SC with that of the general multicomponent SC. The atomic displacement picture, not yet utilized for SCs, is re-introduced in Section 3. The implications of the small mass of hydrogen, separating its effects from those of the heavy metal atom, giving one example and noting the "metallic hydrogen" picture for metal hydrides, are emphasized in Section 4, also providing an essential link to the elemental SC picture (Section 2). Section 5 recounts results for this metallic hydrogen picture applied to five metal hydrides at various pressures, providing specific issues in the understanding of SC in compressed metal hydrides, a main point of the paper. A little recognized analogy of extreme pressure-enhanced SC in elemental lithium, compared to that of metal hydrides, is recounted briefly in Section 6. Section 7 addresses the current search for higher T_c materials by reminding of a single figure of merit picture for understanding and estimating higher T_c materials, with comparison to the ubiquitous two figures of merit picture due to McMillan, elaborated by Allen and Dynes. A Summary of the main points is given in Section 8, followed by an Appendix that provides unpublished information on the analogy (of pressure enhanced T_c) introduced by the atomic displacement picture introduced in Section 3 and used in following sections.

2 | The Conventional Approach

Conventional SC theory for elements is straightforward. Using density functional theory (DFT) methods, calculate the electronic band energies ε_{kn}, determining the Fermi surfaces (FSs), then the phonon frequencies $\omega_{q\nu}$ from sampling through the irreducible Brillouin zone. For each phonon on the mesh, the potential change (below) due to a phonon of wavevector q is calculated, then the electron-phonon matrix elements (functions of $kn, k'n'; q, \nu$) evaluated to integrate $\varepsilon_{k,n}$ and $\varepsilon_{k+q,n'}$ over the FSs $i\varepsilon = \varepsilon_F$. Phonon modes are labeled by wavevector q and branch index ν. One obtains the Eliashberg spectral function $\alpha^2F(\omega)$, from which the electron-phonon coupling (EPC) strength λ is obtained for a *single element* SC as given by McMillan [21]:

$$\lambda = \int \frac{2}{\omega}\alpha^2F(\omega)d\omega \rightarrow \frac{N(0)I^2}{M\omega_2^2}. \tag{1}$$

$F(\omega)$ is the phonon density of states, and $\alpha^2(\omega)$ is the squared EPC matrix element averaged over all phonons of frequency ω. As is well recognized, this expression for λ favors the low frequency range of α^2F. However, high T_c hydrides have λ no larger than very heavy metal elements and alloys known in the 1970s, which have T_c limited to ~10 K, reflecting the importance of the high frequency range of α^2F. Again, the expression above applies only to elemental SCs, in which case the el-ion matrix elements I^2 hides the complication that arises for compounds; for elements it is

$$I^2 = \frac{\sum_{k'n'}\sum_{kn} |<kn|\frac{dV}{d\vec{R}}|k'n'>|^2\delta(\varepsilon_{kn})\delta(\varepsilon_{k'n'})}{\sum_{k'n'}\delta(\varepsilon_{k'n'})\sum_{kn}\delta(\varepsilon_{kn})}, \tag{2}$$

where $V(r,\{\vec{R}\})$ is the electronic potential for ions at positions $\{\vec{R}\}$ and the derivative is respect to displacement of the atom at $\vec{R}$. The double average is over k, n and k', n' over the Fermi surface.

Binary and ternary compounds with more complex unit cells cause an essential complication. Each phonon involves displacement of all atoms, and the preferred method is to calculate the kernel of the matrix element for each phonon, i.e., the potential change, to evaluate the matrix element [22]

$$g_{k,n;k+q,n';q\nu} = \langle k,n|\hat{\varepsilon}_{q\nu}\cdot\frac{dV}{d\hat{\varepsilon}_{q,\nu}}|k+q,n'\rangle \tag{3}$$

only required for states k, n and $k+q, n'$, both on the Fermi surface. Each integrand of the matrix element involves displacements of all atoms involved in phonon q, ν with eigenvector $\hat{\varepsilon}_{q\nu}$, then the scalar product of the eigenvector with the gradient of potential, then evaluation of the matrix element. The potential V is the sum of the pseudopotential and the density dependent potential V^{DFT}, to which we return below. The square $|g_{k,n;k+q,n';q\nu}|^2$ occurs in α^2F. There are so many integrands, i.e., matrix elements, that they have not been analyzed, indeed it is unclear just how they should be analyzed. The squares of these matrix elements are accumulated into $\alpha^2F(\omega)$ involving a sum over all phonons $\{q, \nu\}$, and over k and $k+q$ restricted to the Fermi surface.

To begin to get to the point: each phonon displacement (hence, matrix element) involves contributions from every atom in the cell. The derivative in the above expression is with respect to each phonon eigenvector, and calculation of the matrix element is widely understood by the computational community as costly. The proliferation of indices, sufficient q-mesh grid (see comments in the Appendix), and number of atoms N in the unit cell makes the computational task evident. Alternatively, the finite displacement methods of obtaining force constants in real space can be used, typically extending to (say) the third shell of neighbors. Each of these methods misses the occurrences of Kohn anomalies that may be a primary aspect of the coupling, such as in MgB_2. It is also the case that quantities are no longer simply dependent on $N(0)$ but on how the states are distributed over the various atomic orbital contributions around the FSs. The next section provides a new viewpoint that should provide insight and may be useful in electron-phonon coupling codes.

3 | Reviving the "Enatom"

There might be a more instructive way. Each "kernel" of the phonon matrix element Equation (3) involves the first order displacement of every atom in the unit cell. These responses to phonon displacements are calculated over and over for each wavevector q in Quantum Espresso [51]. This repetitive calculation of each atom's linear response suggests looking for an alternative, for which the "enatom" may be useful as well as the main intent to provide deeper understanding.

Textbooks teach that separation of a solid's charge density into contributions from separate atoms is subjective, even arbitrary. This result is based on some history of the desire. Ziman intro-

duced the pseudoatom in the context of weak pseudopotentials, where the formalism can be expanded in powers of the pseudopotential, and at first order a pseudoatom picture arises [23]. A more nuanced construction of the associated pseudopotentials and resulting density was articulated by Heine and Abarenkov [24], with several further developments in pseudopotential theory, not specifically related to a pseudoatom picture. In constructing stronger pseudopotentials for transition metal atoms, Moriarty introduced a pseudoatom, a first approximation to the atomic density [25].

While true as stated – the static crystal density cannot be separated uniquely into single atom contributions – six decades ago this statement was shown to address too specific a question, that is, too specific a system (the static lattice). Considering a solid (let's say a crystal, though that is not necessary for the theorem), Ball demonstrated using infinitesimal atomic displacements and translational invariance that such a separation is possible [26, 27] and unique, with physical consequences. His initial interest was in the density and the consequences of density distortions. Ball's ideas were adapted in the quasi-atom approach of Falter and collaborators [28] applied to density response, phonon spectra, and electron-phonon coupling, and were adapted by Ball and Srivistava [29] to total energy calculations. The interest here is not on the enatom density but on the corresponding enatom potential [30] and its application to electron-phonon coupling.

The displacement of a single atom $\vec{R}_j$ in a crystal with density $n(\vec{r},\{\vec{R}\})$ depending on the atomic positions deviating mildly from equilibrium positions $\{\vec{R}^\circ\}$ gives rise to a vector field, which can be decomposed into its irrotational and divergenceless fields as

$$\frac{\partial n(\vec{r};\{\vec{R}\})}{\partial \vec{R}_j} = -\nabla\rho_j(\vec{r}-\vec{R}_j^\circ) + \nabla\times\vec{B}_j(\vec{r}-\vec{R}_j^\circ). \tag{4}$$

This expression is a purely mathematical statement: a vector field can be decomposed into the gradient of a scalar function ρ_j and the curl of a vector function $\vec{B}_j$, with each reasonably measured with respect to undisplaced position R_j° of the atom that was displaced. Ball showed, in a very simple demonstration (incorporating the infinitesimal displacement of the crystal as a whole) with a profound result, that (1) the lattice sum of the scalars ρ_j that move rigidly replicates the periodic density, giving a unique decomposition of the density into a sum of atomic contributions. In addition, (2) the lattice sum of the vector deformations ("backflows") $\nabla\times\vec{B}_j$ vanishes. This pair of quantities, both the rigid and backflow parts, were given the name [32] "enatom" ("en" meaning in Greek "to cut from within") to distinguish it from several previous uses of "pseudoatom" or "quasi-ion" for related but either weak pseudopotential or sublattice applications, as related in an early paper [30].

Because it is central to the following description, this identical separation (which applies to any function of $\vec{r}$ that is parametrically dependent on the atomic positions) is displayed here; the rigidly displaced pseudopotential is straightforward. Explicitly for the full DFT electronic potential $V^{DFT}(\vec{r};\{\vec{R}\})$ (Hartree plus exchange-correlation):

$$\frac{\partial V^{DFT}(\vec{r};\{\vec{R}\})}{\partial \vec{R}_j} = -\nabla v_j(\vec{r}-\vec{R}_j^\circ) + \nabla\times\vec{W}_j(\vec{r}-\vec{R}_j^\circ). \tag{5}$$

This defines the rigid $v_j(r-R_j^\circ)$ and backflow (or deformation) $\vec{W}_j(r-R_j^\circ)$ fields of the first order change in potential, which is related through the dielectric function to the enatom density [30]. As for the density $n(r;R)$, this rigid part is a precise decomposition of the total potential V^{DFT}, and the lattice sum of undisplaced backflow parts $\nabla\times\vec{W}_j$ vanishes, written explicitly here for emphasis

$$\sum_j v_j(\vec{r}-\vec{R}_j^\circ) = V^{DFT}(\vec{r};\{\vec{R}^\circ\}),$$
$$\sum_j \nabla\times\vec{W}_j(\vec{r}-\vec{R}_j^\circ) = 0. \tag{6}$$

This derivative in Equation (5) is of course the gradient that appears in the electronic matrix element g or I along with the gradient of the pseudopotential, which is available in current codes. Note that $\vec{W}_j$, like $\vec{B}_j$ above, is only defined to within a gauge, i.e., the gradient of a scalar function, but $\nabla\times\vec{W}_j$ is unique (and physical) and that is what is used in the EPC matrix elements. It is natural to discuss $\vec{W}_j$ in the divergenceless gauge.

This gradient, the matrix element kernel, has a limited range due to the strong local screening in a metal. It can be obtained readily from DFT calculations in a supercell of reasonable size (viz. a 3× 3× 3 supercell, or less for larger primitive cells). Either DFT perturbation theory can be used to obtain the gradient (using formalism for an infinitesimal displacement) or from a few finite displacements on a reasonable mesh, which are relatively quick calculations even for a few dozen atoms in the cell. If desired, and likely to be important for understanding, the Helmholtz construction [30], expressed simply in a Fourier expansion, can provide these rigid v_j and backflow $\vec{W}_j$ components of the change in potential. The Helmholtz procedure relies only on the analyticity of the quantities, which is ensured by their representation in code by a finite Fourier expansion over reciprocal lattice vectors. At this stage this procedure may appear only like a change in representation of the derivative, from phonon to individual atoms. For the compressed metal hydrides, it provides an essential simplification and likely insight, as will be described.

4 | The Small Mass of Hydrogen

The foregoing separation of the potential holds for any solid, but these derivatives provide the kernel of the EPC matrix element. The important feature discussed here relates to the mass difference between H and the metal(M), well recognized but not taken full advantage of. Because of this mass difference $F(\omega)$ and $\alpha^2F(\omega)$ divide into two regimes separated by a gap, sometimes a substantial one. Even for SH_3 with smaller mass difference than most (32:1), the contributions are divided into a low frequency (acoustic) spectrum that is, to excellent approximation, associated with the metal S, and a higher frequency (optic) region involving dominantly H vibrations. This separation is much more the case

for La in LaH_{10}, with its 139:1 mass ratio because the heavy atom is unable to follow the rapid H motion.

This observation is reminiscent of the "double Born approximation" of Onuorah *et al.* [33] for muons in solids ($m_\mu = 207 m_e$) – electrons respond almost adiabatically to the muon position, while in turn the muon responds quasi-adiabatically to the heavy atoms. In hydrides, H responds roughly adiabatically to the position of the heavy metal atom. Thus the separate H and metal phonon eigenvectors form an approximately orthonormal eigensystem of the respective vibrations, which becomes useful in the formalism.

Because α^2F separates, it is also true of λ and the frequency moments [31], and I^2 is an atomic property (as is the mass), so it follows that

$$\lambda = \lambda_M + \lambda_H; \quad \lambda_j = N_j(0) I_j^2 / M_j \omega_{2,j}^2. \tag{7}$$

It is then only necessary to divide $N(0)$ into contributions from each atom, a somewhat subjective process but one that won't differ greatly amongst practitioners and should be done such that the atomic contributions sum to $N(0)$. This separation is not possible for conventional intermetallic metals, where atomic character is mixed throughout α^2F.

This separation of λ is broadly recognized, and the partial integral over $2\alpha^2F(\omega)/\omega$ is standardly plotted as an integral over the integrand up to a limit of ω, providing $\lambda(\omega)$ that reveals the contribution from each regime, i.e. each atom. Typically the metal contribution is 15–20% of λ. This low frequency contribution is sometimes credited with providing the last increment to λ that boosts T_c significantly. Such is *not* the case, as described in the following section.

The first study for hydrides of this separation was presented by Papaconstantopoulos et al. [6] who applied the rigid atomic sphere model (known as the "rigid muffin tin approximation") of Gaspari and Györffy [34]. This model was derived specifically to calculate the atomic I_j^2 for individual atoms, and the model is very useful for close packed transition metals. It becomes more approximate for superconductors where the change in potential becomes less strongly local, or directional in character.

The result for SH_3 is shown in Figure 1, along with $\eta_j = N(0)_j I_j^2$, for each of the two atoms. The strong increase in I_H^2 (hence η_H) under pressure is surprising. After all, increasing pressure, hence increasing density, might be expected to increase screening, thus reducing the change in potential with motion and decreasing I_H^2. However, static screening depends largely on $N(0)$. Band broadening under pressure will decrease $N(0)$ and possibly screening, thereby enhancing I^2 when calculated self-consistently. Additionally, it is the density of states per unit volume that is comparable among materials, and the volume decreases with pressure, giving some offset to the band broadening.

These competing expectations require more direct study. This calculated increase in I^2 (for both atoms) is dominant in SH_3, so the expectation that H, without any core to screen, should be a stronger scatterer than typical metals (with substantial cores, hence effective pseudopotentials), seems unclear (within the

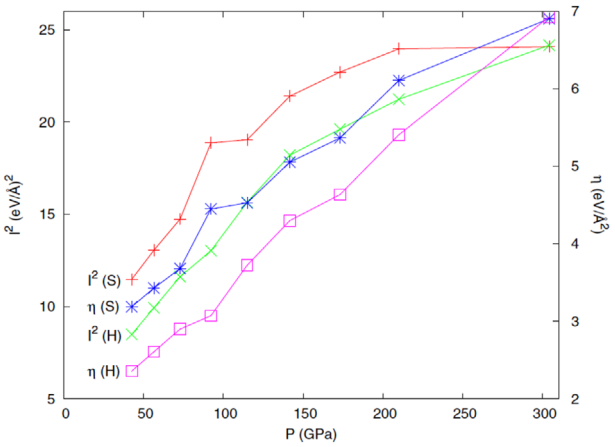

FIGURE 1 | Pressure dependence of the separate S and H values for I^2 and $\eta = N(0)I^2$, calculated from the Gaspari-Györffy multiple scattering expression [34]. The increase under pressure is due almost entirely to the increase of I^2 (for each atom). The physical regime for SH_3 is from 160 GPa and above, where the increase in I_H^2 is 25% by 300 GPa. The figure is reproduced from Ref. [6]. Copyright: American Physical Society.

Gaspari-Györffy model). However this superconductor is not the best to judge because E_F lies very near the peak of a sharp and narrow van Hove singularity [35], (vHs) where behavior under pressure is uncertain to estimate. Also, additional physics arises, including electron velocities vanishing (leading to non-adiabatic effects) and the electron scattering by phonons $\varepsilon_k + \omega_q \rightarrow \varepsilon_{k+Q}$ involves scattering across the vHs, i.e. the density of states N(ε) as well as the velocities results in more complex behavior.

5 | Metal and Hydrogen Atoms Separately

The focus therefore turns to hydrogen specifically

$$T_c = F(\omega_{log,H}, \omega_{2,H}, \lambda_H);\ \lambda_H = \frac{N_H(0) I_H^2}{M_H \omega_{2,H}^2}, \tag{8}$$

with analogous expressions for the metal with M subscripts (which alone gives a vanishing T_c). With the other factors being calculated (with the known mass) the property that is unknown is I_H^2, and it has attracted almost no attention in hydrides beyond that mentioned in the previous section. The M-H separation of λ and the frequency moments allows a conceptual exercise: what would T_c be if only the M, or only H, contributions were present? Note that the sum of these would not add to the true T_c due to the nonlinearities that are involved, but the sum is not of interest.

Quan *et al.* [36] considered five compressed metal hydrides – SH_3, LaH_{10}, YH_{10}, CaH_6, MgH_6 – each at a few different pressures, and studied the separate metal and hydride contributions to T_c. The results for I_H^2 (the other quantities are calculated or known) are presented in Figure 2. To summarize: when the metal contribution to α^2F was discarded, T_c was *essentially unchanged* (and the tiny M contribution to T_c could be negative as well as positive, because ω_{log} was decreased). Instances of this effect are quantified in the tables of Quan *et al.* [36] Specifically, the decrease in λ by ignoring the M contribution, which tends to decrease T_c, is canceled by the increase in ω_{log} and ω_2, which

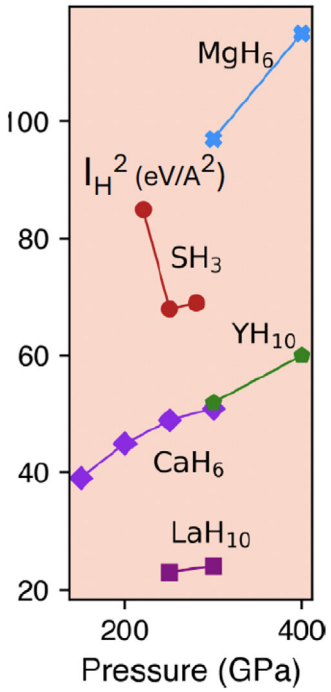

FIGURE 2 | Pressure dependence of I_H^2 (hydrogen alone) for five metal hydrides at assorted values of pressure, extracted from Equation 7 when all the other factors are calculated. The factor of five spread is unexpected, and the factor of two between CaH_6 and isovalent, isostructural MgH_6 at 300 GPa raises questions. The highest T_c metal hydride at this time, LaH_{10}, has the lowest I_H^2 of this group, without any explanation yet. The figure is reproduced from Ref. [36]. Copyright: American Physical Society.

increase T_c. When the H contribution to α^2F was deleted, of course the metal atom $\lambda_M \sim 0.15 - 0.25$ on its own gives no superconductivity. This picture aligns well with the original concept of Ashcroft [37] – metallic hydrogen – that high H frequencies and moderate screening would lead to high values of T_c. Many numerical values of related quantities are given in the tables in Ref. [36].

The conclusion is that ignoring the M contribution does not affect T_c, i.e. these metal hydrides are simply *metallic hydrogen superconductors*, with the metal contribution providing stability of the compound but confusing the source of T_c. This picture is also close to the second vision of Ashcroft [38], using H-containing molecules to provide pre-compressed reservoirs of hydrogen and resulting hydrogen superconductivity. So far, high symmetry structures have provided the successes, though that is a separate subject. Turning attention now specifically to the H parameters should enable essential quantitative input into the high values of T_c.

The results of Quan *et al.* [36] give a sharp indication of the next level of questions to be addressed. The derived values of I_H^2 versus pressure, presented in Figure 2, is startling in a few respects. The dominant trend is toward higher values as pressure increases, as for the GG values [34] of I_H^2 for SH_3. Unexpected is that the strengths of scattering I_H^2 differ considerably amongst the five hydrides, especially considering that SH_3 and LaH_{10} are the first two confirmed high T_c members, both having T_c of 200 K or greater. Overall the values differ by a factor of five over the range 200–400 GPa for the cases that were calculated.

It is noteworthy that the highest T_c hydride LaH_{10} 'scores low' on this competition, very surprising considering its highest confirmed T_c~250–260 K. Another surprise is the factor of two difference between CaH_6 and MgH_6, which needs an explanation, similarly for LaH_{10} and YH_{10}. A path forward that might provide the explanation is the implementation and analysis of the enatom potential and matrix elements. The non-monotonic behavior of SH_3 is likely because E_F lies very near the top of a van Hove singularity [35], (vHs) which makes pressure effects delicate [especially N(0)] and requires additional theory (the phonons scatter electrons from a region below E_F, below the peak, to above above the peak, requiring corrections to the usual constant $N(E) \approx N(0)$ treatment) and computational precision for accurate predictions (an example is given in the Appendix).

6 | Previous Pressure Enhancement of T_c

6.1 | Lithium as a High T_c Superconductor

Considering the large increase in metal hydrides with pressure, an analogy can be considered. Metal hydride superconductivity increased from ~10 K (PdH) at ambient in the 1970s to 250–260 K around 200 GPa in LaH_{10} around 2020, a factor of 25. There is a related but yet more extreme example. Lithium, finally discovered to be a 180 μK superconductor [39] in 2007, when squeezed to 35 GPa achieves ~20 K superconductivity - around five decades of increase [40–42]. This increase, to the highest T_c for any element at the time, is almost unbelievable for a weak pseudopotential, nearly free electron monovalent metal. The story is an instructive one, see the original papers for the full story [43, 44].

In short, pressure transforms bcc Li to fcc Li, upon which the spherical bcc Fermi surface develops necks across the L point (just like the monovalent Cu Fermi surface) where the electron velocity drops by more than a factor of two, and strong and very localized nesting features [45–47] arise, resulting in unexpected and strong fine structure in the q dependence of the phonon linewidths (nesting function with electron-phonon matrix elements inserted) and their associated contribution to α^2F and T_c. Not a large N(0), but a comparatively large I^2, and α^2, that was difficult to converge even with very fine k- and q-meshes, a few more details are given in the Appendix. More complex Fermi surfaces will enhance such occurrences, but Li shows fine structure in q can happen for even the simplest of Fermi surfaces.

6.2 | Glimpse of the Li Enatom

At around the same time the lithium enatom was calculated, as a demonstration of the method, by Kunstmann *et al.* [32, 48] for the simple metals Li and Al (T_c = 1.2 K) at ambient for a few pressures, in part because these atoms could be represented by local pseudopotentials and also because they display different behavior under pressure. The very large T_c increase in Li is described above. For Al, T_c decreases under pressure, with unreachably low temperatures above 20 GPa.

Not surprisingly for these nearly free electron metals (except that beyond expectation one (Li) could display high temperature superconductivity), the rigid potentials, restricted by symmetry to be cubic, were found to remain close to spherical under pressure. (For Li the rigid density included a *negative value* in the region of second and third neighbors, such behavior is allowed.) The non-spherical components of the rigid potential could be identified, and also the Friedel oscillations in the rigid potential. With no surprise, the backflow potentials, restricted to have the cubic symmetry of a vector field and whose lattice sum must vanish, seemed (without much to compare to) to be small. Seemingly, matrix elements (not computed) would be dominated by the displacements of the spherical rigid potentials v_j and pseudopotential, with little effect from the deformation potential. Comparison of the rigid potentials at different pressures revealed no surprises, suggesting that evolution of the FS (shape and velocities) is responsible for the increase in I^2. A glimpse of the deformation density and potential of Li at 35 GPa (T_c~20 K) is given in the Appendix.

7 | Searching for Higher T_c

There is an auxiliary purpose of this paper beyond understanding of the increase of T_c: to contribute to the search, in progress by many groups, to discover and predict competently even higher T_c hydrides under pressure, but ideally at ambient conditions. A given higher T_c hunt might have an emphasis on larger $N(0)$ or λ, keeping in mind that this direction invites other instabilities. Pushing strong coupling to higher frequencies might be a different goal. These two figures of merit for T_c – λ and a frequency moment $<\omega>$ – have dominated the discussion since the time of McMillan's Equation 1.

7.1 | A Single Figure of Merit

This tradeoff was addressed five decades ago by Leavens and Carbotte (LC) [49, 50], who were surveying the strong coupling materials of the 1970s in terms of Eliashberg theory. As a different measure of the underlying influence of $\alpha^2F(\omega)$, which is what determines T_c, they found that a different focus rather than λ and $g(\omega) = (2/\lambda)\alpha^2(F(\omega)/\omega$ (the normalized shape function) showed promise. Their focus was on the area $\mathcal{A}$ under $\alpha^2F(\omega)$, rather than λ and moments of $g(\omega)$. This area gave a simple and impressively good correlation with the experimental data at the time. Their fit to data gave (temperature and frequency will be expressed in the same energy units, i.e. $k_B = 1 = \hbar$)

$$T_c^{LC} = 0.148\mathcal{A} = 0.074\,\omega_1\lambda \tag{9}$$

as a good representation of T_c. The constant would depend somewhat on μ^*, and the last expression uses the first moment of Allen and Dynes. One interpretation of $\mathcal{A}$ is that this area is the product of the average of α^2F over the full interval $[0, \omega_{max}]$ times the length ω_{max} of the interval. Roughly speaking, λ is the measure of the strength of α^2F, while ω_1, which is independent of the strength of α^2F but depends only on its shape and extent, is the measure of the spread of the coupling. The distribution over frequencies in this interval would play no discernible part. Restating, the low frequency part λ would be balanced by the higher frequency measure ω_1. One implication is that increasing one while keeping the other constant would increase T_c, similar to the usual picture but differing in numerical detail. Since $M\omega_2^2$ is independent of mass for a harmonic elemental solid (so $M\omega_1^2$ is roughly so as well), the LC expression has an $M^{-1/2}$ mass dependence, following the standard isotope shift for elemental SCs. As always, compounds are more complex – atomic contributions are mixed together in all quantities.

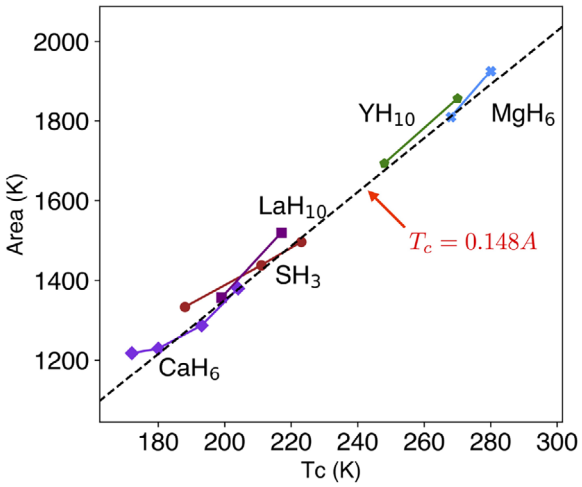

FIGURE 3 | A scatterplot of the area $\mathcal{A}$ versus T_c for the five binary hydrides at the various pressures that were calculated by Quan and Pickett [36]. Note that T_c and $\mathcal{A}$ are calculated from the H vibrational spectrum of α^2F. The strong correlation is evident. The slope of 0.148 denotes the Leavens-Carbotte line for strong coupled intermetallics existing in 1974. The figure is reproduced from Ref. [36]. Copyright: American Physical Society.

7.2 | Application to Hydrides

One can then ask whether this $\mathcal{A}$ figure of merit has relevance in compressed hydrides. The correlation between $\mathcal{A}$ and T_c for the five compressed hydrides shown in Figure 2 is provided in Figure 3. Recall that only the H part of α^2F is used in the results in both figures, the metal hydrides have become more simply "hydride superconductors." The excellent correlation is evident. Moreover, the proportionality (slope of the line) is the same as for the 1970s elemental superconductors and 21st century compressed metal hydrides (once the metal contribution is neglected). This equivalence in value and slope is remarkable: the hydrides have T_c up a factor of 25 or more higher, "because" the area $\mathcal{A}$ is that much larger. This correlation further suggests that T_c for known compressed metal hydrides is far from optimal: $N_H(0)$ or/and I_H^2 need to be increased for higher T_c.

The importance of $N(0)$, without focus on $N_H(0)$, has always been forefront, the importance of I_H^2 and $N_H(0)$ instead of frequencies now assumes more relevance. Coupling throughout the frequency spectrum of α^2F, with amplitude as large as possible and frequencies extending as high as possible, seems to be the key to high T_c in compressed metal hydrides as the correlation also suggested for the 1970s high T_c materials. Possibly similar correlations may apply to ambient condition hydrides as well if

the H modes are separated from those of the metal(s). Ambient pressure possibilities are currently being actively sought, viz. Mg_2IrH_6 [52], but with limited success so far in the synthesis of predicted candidates.

The LC expression T_c versus $\mathcal{A}$ is somewhat reminiscent of the strong coupling limit of T_c within Eliashberg theory established by Allen and Dynes (AD) [31], obtained formally as

$$T_c^{max,AD} = 0.18\,\omega_2\sqrt{\lambda} = 0.18\sqrt{\frac{N(0)I^2}{M}}, \tag{10}$$

note no explicit dependence on frequency moments. The LC expression can be written (for an element)

$$T_c^{LC} = 0.074\frac{\omega_1}{\omega_2}\frac{N(0)I^2}{M\omega_2}, \tag{11}$$

thus scaling differently with $\eta = N(0)I^2$ but with the same (correct) scaling with mass ($\omega_1 \propto M^{-1/2}$). The LC expression, not intended for very strong coupling, can be regarded as a linearization of $T_c(\lambda)$ in a regime that is still far from the AD limiting regime. This view would then suggest that current compressed hydrides are still well below the limiting regime of T_c, as indeed the AD equation for T_c indicates.

7.3 | A Differential Viewpoint

To repeat: the LC relation indicates that the importance is the mean magnitude of α^2F over as large a range as possible. Those properties determine $\mathcal{A}$ and thus T_c (in their regime of applicability), in neither case is there any importance of any explicit frequency distribution. Can this (phenomenological) view be reconciled with the rigorous result of Bergmann and Rainer (BR) from Eliashberg theory that suggests a different viewpoint? [53] BR calculated for a number of known α^2F functions the functional derivative

$$\mathcal{D}(\omega) \equiv \frac{\delta T_c[\alpha^2F, \mu^*]}{\delta\alpha^2F(\omega)}, \tag{12}$$

which gives the change in T_c that will result from an extra increment $\Delta\alpha^2F$ at ω. This is a material dependent function, i.e. dependent on α^2F but finally reflecting little if any real dependence on material (for their sample). This function is linear at low ω (indicating a poor choice of frequency region for increasing T_c), it peaks at a value δ_m, just above $\omega \sim 2\pi T_c$ (more precisely, around $6.5T_c$), then decreasing rather slowly beyond. Thus if strength can be increased at high frequency it is not so important at what frequency, but it is better than adding at low frequency, the separation occurring at δ_m, the optimal position.

The resolution of this difference of AD and LC pictures is (at least) twofold. First, the rigorous results of BR for the derivative (essentially the same for several elemental SCs when scaled as ω/T_c) were for strong coupled SCs with T_c up to 15 K, mostly heavy metals. Different classes, with different distributions of $\alpha^2F(\omega)$, might show different behavior. Second is that one usually cannot simply add (or delete) new phonons with coupling to a material. However, one can imagine altering a material to give a shift in $\Delta(\omega)$ weight in specific regions of frequency, viz. by substituting (similar) atoms, or by external means (strains, pressure, or boundaries).

This question was elaborated by Camargo-Martínez *et al.* [54], who evaluated α^2F and $\mathcal{D}(\omega)$ for SH_3 at pressures from 215 GPa down to 155 GPa, where their (harmonic) T_c values increased from 138 K to 203 K, correlating reasonably with the experimental data. Their peak position δ_m of $\mathcal{D}(\omega)$ occurred near $7k_BT_c$ (versus $6.5k_BT_c$ for BR), but otherwise showed the same frequency dependence. Upon lowering pressure, the lower frequency peak of H vibrations shifted downward and coincided with δ_M at 155 GPa, and the increase in T_c correlated well with the shift in $\mathcal{D}(\omega)$ as pressure was lowered. Comparing values of $\mathcal{A}$ is not possible (without certain projections) because the S and lower H vibrations become mixed at the lower pressures, in spite of the factor of 32 difference in atomic masses.

8 | Summary

The title is "why compressed hydrides are such high T_c superconductors;" well, it is due to the hydrogen scattering of electrons on the Fermi surface. Any more than this observation is yet to be understood. The missing information relates to the strength and character of this scattering. The starting point of this Perspective lies in the McMillan expression for λ for *elemental* superconductors. The factors of $N(0)$ and $M\omega_2^2$ are standard outputs of calculations. The electron-ion scattering matrix elements I^2 are almost unstudied for hydrides. The second step is to take advantage of the large mass difference between metal M and H (widely understood), whereupon scrutiny reveals that the contribution of M for T_c is vanishingly small, learned from a set of five high T_c hydrides at a few pressures – the metal hydrides are in effect *elemental* H superconductors.

With this information, focus is on the scattering I_H^2 of the H atom. The enatom approach provides naturally the H scattering potential $\nabla_{R_H}V$ for analysis in real space, which is then followed by calculation and analysis of the Fermi surface and the resulting scattering, to form an understanding why the H Fermi surface scattering strength increases strongly under pressure. It may be the potential change (a screening effect) or a Fermi surface effect (viz. nesting in regions of strong coupling processes), or a combination of the two.

The analogy of Li has been provided: starting from a sub-mK value, its T_c is increased by five orders of magnitude at 35 GPa, to around 20 K. Its scattering (enatom) potential appears to change normally with volume, with the increase in coupling caused by change in Fermi surface shape, velocities, and orbital character. This example provides the sorts of effects to be studied in I_H^2 and T_c in metal hydrides. Admittedly, to change this nearly non-superconducting metal into a 20 K SC requires a relatively modest increase in λ and frequencies.

Finally, three viewpoints related to considering what might provide some focus on searching for and predicting higher T_c superconductors are discussed. These are the McMillan-Allen-Dynes parameterization of T_c in terms of two figures of merit (λ and a frequency moment), the Leavens-Carbotte empirical

observation of a single figure of merit that correlates linearly with T_c (the area under α^2F), and the functional derivative of Bergmann and Rainer $\delta T_c/\delta\alpha^2F(\omega)$ that points to an optimal frequency regime for focusing coupling, a regime that scales simply with T_c. These three pictures encourage the practice of keeping all three in mind, without undue focus on a single one.

While higher T_c superconductors in the compressed metal hydride families continue to be sought, much of the effort has turned to higher T_c materials at ambient pressure, hence more thoroughly characterized and perhaps applied. The ideas presented here should apply to hydrides at ambient. The other main direction of search has been on light and strongly (covalently) bonded metals in the B-C-N families. While the current focus on an elemental I^2 will not apply directly there – frequency ranges will be shared by two or more atoms, and the generalization of I^2 includes cross terms – the strong scattering processes in those materials will need to be studied and there may be a useful generalization of the ideas presented in this paper.

The enatom picture has other applications involving phonon- or strain-related transport. One example is the response of the electronic states and band energies to strains or pressure. Khan and Allen proved [55], after a few decades of study by prominent theorists, that the strain deformation potential – shift in ε_k due to a strain – is given by the band diagonal, $q = 0$, matrix elements of the enatom potential appended by a simple kinematic quantity that accounts for the distortion of the Brillouin zone. Likely there are other applications of the enatom potential and associated density in the many manifestations of transport theory.

Acknowledgements

This contribution was provided in memory of Mikhail Eremets, the leader of the high pressure group at MPI Mainz that discovered the 200K superconductor SH_3 (and LaH_{10} afterwards). Mikhail was a leader in the field of high pressure physics, a thoughtful coauthor [56], a conscientious guide for lab tours (twice) for this author, a valued friend, and an exemplary member of his scientific community. A visit to Liverpool hosted by Michael Ball in 1976 confirmed my decision to keep this 'enatom' picture in mind. My coauthors on earlier work on the enatom of Li and Al, Jens Kunstmann and Lilia Boeri, deserve acknowledgment for their collaboration in the midst of their primary research responsibilities. I also acknowledge the construction of a picture of coupling in Li, perhaps a resolution but not quite of publication convincability, by Jan Kuneš, of the superconductivity of Li resulting from a convergence of electron $2p$ character of matrix elements coinciding with strong nesting regions on the Fermi surface. Input from Christoph Heil has proven quite useful for this manuscript.

Conflict of Interest

The authors declare no conflict of interest.

Data Availability Statement

Data sharing is not applicable to this article as no new data were created or analyzed in this study.

References

1. A. P. Drozdov, M. I. Eremets, and I. A. Troyan, "Conventional Superconductivity at 190 K at High Pressures," *arXiv:1412.0460* (2014).

2. A. P. Drozdov, M. I. Eremets, I. A. Troyan, V. Ksenofontov, and S. I. Shylin, "Conventional Superconductivity at 203 Kelvin at High Pressures in the Sulfur Hydride System," *Nature* 525 (2015): 73–76.

3. M. Einaga, M. Sakata, T. Ishikawa, et al., "Crystal Structure of the Superconducting Phase of Sulfur Hydride," *Nature Physics* 12 (2016) 835–838. .

4. D. Duan, Y. Liu, F. Tian, et al., "Pressure-induced Metalization of Dense $(H_2S)2H_2$ with High-T_c Superconductivity," *Scientific Reports* 4 (2014): 6968.

5. Y. Li, J. Hao, H. Liu, Y. Li, and Y. Ma, "The Metalization and Superconductivity of Dense Hydrogen Sulfide," *Journal of Chemical Physics* 140 (2014): 174712.

6. D. A. Papaconstantopoulos, B. M. Klein, M. J. Mehl, and W. E. Pickett, "Cubic H_3S Around 200 GPa: An Atomic Hydrogen Superconductor Stabilized by Sulfur," *Physical Review B* 91 (2015): 184511.

7. I. Errea, M. Calandra, C. J. Pickard, et al., "High-pressure Hydrogen Sulfide from First Principles: A Strongly Anharmonic Phonon-mediated Superconductor," *Physical Review Letters* 114 (2015): 157004.

8. N. Bernstein, C. S. Hellberg, M. D. Johannes, I. I. Mazin, and M. J. Mehl, "What Superconducts in Sulfur Hydrides Under Pressure and Why," *Physical Review B* 91 (2015): 060511(R).

9. R. Akashi, M. Kawamura, S. Tsuneyuki, Y. Nomura, and R. Arita, "First-Principles Study of the Pressure and Crystal-structure Dependences of the Superconducting Transition Temperature in Compressed Sulfur Hydrides," *Physical Review B* 91 (2015): 224513.

10. J. A. Flores-Livas, A. Sanna, and E. K. U. Gross, "High Temperature Superconductivity in Sulfur and Selenium Hydrides at High Pressure," *European Physical Journal B: Condensed Matter and Complex Systems* 89 (2016): 63.

11. Y. Quan and W. E. Pickett, "van Hove Singularities and Spectral Smearing in High Temperature Superconducting H_3S," *Physical Review B* 93 (2016): 104526.

12. I. Errea, M. Calandra, C. J. Pickard, et al., "Quantum Hydrogen Bond Symmetrization in the Superconducting Hydrogen Sulfide System," *Nature* 533 (2016): 81- 84..

13. H. Liu, I. I. Naumov, R. Hoffmann, N. W. Ashcroft, and R. J. Hemley, "Potential High-Tc Superconducting Lanthanum and Yttrium Hydrides at High Pressure," *Proceedings of the National Academy of Sciences* 114 (2017): 6990–6995.

14. A. P. Drozdov, V. S. Minkov, S. P. Besedin, et al., "Superconductivity at 215 K in Lanthanum Hydride at High Pressures," *arXiv:1808.07039*.

15. A. P. Drozdov, P. P. Kong, V. S. Minkov, et al., "Superconductivity at 250 K in Lanthanum Hydride Under High Pressures," *arXiv:1812.01561*.

16. M. Somayazulu, M. Ahart, A. K Mishra, et al., "Evidence for SuperConductivity above 260 K in Lanthanum Superhydride at Megabar Pressures," *Physical Review Letters* 122 (2019): 027001.

17. F. Peng, Y. Sun, C. J. Pickard, et al., "Hydrogen Clathrate Structures in Rare Earth Hydrides at High Pressures: Possible Route to Room-temperature Superconductivity," *Physical Review Letters* 119 (2017): 107001.

18. P. Kong, V. S. Minkov, M. A. Kuzovnikov, et al., "Superconductivity up to 243K in the Yttrium-Hydrogen System Under High Pressure," *Nature Communications* 12 (2021): 5075.

19. E. Snider, N. Dasenbrock-Gammon, R. McBride, et al., "Synthesis of Yttrium Superhydride Superconductor With a Transition Temperature up to 262 K by Catalytic Hydrogenation at High Pressures," *Physical Review Letters* 126 (2021): 117003.

20. W. E. Pickett, "Colloquium: Room Temperature Superconductivity: the Roles of Theory and Materials Design," *Reviews of Modern Physics* 95 (2023): 021001.

21. W. L. McMillan, "Transition Temperature of Strong-Coupled Superconductors," *Physical Review B* 167 (1968): 331–344.

22. F. Giustino, "Electron-Phonon Interactions from First Principles," *Reviews of Modern Physics* 91 (2016): 019901.

23. J. Ziman, "The Method of Neutral Pseudo-Atoms in the Theory of Metals," *Advances in Physics* 13 (1964): 89–138.

24. V. Heine and I Abarenkov, "A New Method for the Electronic Structure of Metals," *Philosophical Magazine* 9 (1964):451–465.

25. J. A. Moriarty, "Zero-Order Pseudoatoms and the Generalized Pseudopotential Theory," *Physical Review B* 10 (1974): 3075–3091.

26. M. A. Ball, "General Theory of the Effect of Ionic Motion on Charge Density," *Journal of Physics C* 8 (1975): 3328–3340.

27. M. A. Ball, "The Effect of a Phonon on the Charge Density of a Crystal," *Journal of Physics C* 10 (1977): 4921–4934.

28. C. Falter, W. Ludwig, M. Selmke, and W. E. Pickett, "A Quasi-Ion Approach to Lattice Dynamics and Electron-Phonon Interaction With Applications," *Journal of Physics C* 20 (1987): 501–520. See references therein for their preceding works on the quasi-ion approach.

29. M. A. Ball and G. P. Srivastava,, "The Derivation of Pseudoatom Information in Germanium from Total-Energy Calculations," *Journal of Physics: Condensed Matter* 4 (1992): 1947–1958.

30. W. E. Pickett, "The Generalized Pseudoatom Potential in Solids: Relation to Screening and Lattice Dynamics," *Journal of Physics C* 12 (1979): 1491–1503.

31. P. B. Allen and R. C. Dynes, "Transition Temperature of Strong-Coupled Superconductors Reanalyzed," *Physical Review B* 12 (1975): 905–922.

32. J. Kunstmann, L. Boeri, and W. E. Pickett, "Linear Response Separation of a Solid into Atomic Constituents: Li, Al, and Their Evolution Under Pressure," *Physical Review B* 75 (2007): 075107.

33. I. J. Onuorah, P. Bonf, R. De Renzi, et al., "Quantum Effects in Muon Spin Spectroscopy Within the Stochastic Self-Consistent Harmonic Approximation," *Physical Review Materials* 3 (2019): 073804.

34. G. Gaspari and B. L. Györffy, "Electron-phonon Interactions, *d* Resonances, and Superconductivity in Transition Metals," *Physical Review Letters* 28 (1972): 801–806.

35. S. S. Ghosh, Y. Quan, and W. E. Pickett, "Strong Particle-Hole Asymmetry in a 200 Kelvin Superconductor," *Physical Review B* 100 (2019): 094521.

36. Y. Quan, S. S. Ghosh, and W. E. Pickett, "Compressed Hydrides as Metallic Hydrogen Superconductors," *Physical Review B* 100 (2019): 184505.

37. N. W. Ashcroft, "Metallic Hydrogen: A High-Temperature Superconductor?," *Physical Review Letters* 21 (1968): 1748–1749.

38. N. W. Ashcroft, "Hydrogen Dominant Metallic Alloys: High Temperature Superconductors?," *Physical Review Letters* 92 (2004): 187002.

39. J. Touriniemi, K. Juntunen-Nurmilaukas, J. Uusvuori, E. Penttti, A. Salmela, and A. Sebedash, "Superconductivity in Lithium Below 0.4 Millikelvin at Ambient Pressure," *Nature* 447 (2007): 187–189.

40. K. Shimizu, H. Ishikawa, D. Takao, T. Yagi, and I. Amaya, "Superconductivity in Compressed Lithium at 20K," *Nature* 419 (2002): 597–599.

41. V. V. Struzhkin, M. I. Eremets, W. Gan, H.-K. Mao, and R. J. Hemley, "Superconductivity in Dense Lithium," *Science* 298 (2002): 1213–1215.

42. S. Deemyad and J. S. Schilling, "Superconducting Phase Diagram of Li Metal in Nearly Hydrostatic Pressures up to 67 GPa," *Physical Review Letters* 91 (2003): 167001.

43. D. Kasinathan, J. Kuneš, A. Lazicki, et al., "Superconductivity and Lattice Instability in Compressed Lithium from Fermi Surface Hot Spots," *Physical Review Letters* 96 (2006): 047004.

44. D. Kasinathan, K. Koepernik, J. Kuneš, H. Rosner, and W. E. Pickett, "Origin of Strong Coupling in Lithium Under Pressure," *Physica C* 460–462 (2007): 133–136.

45. G. Gilat and L. J. Raubenheimer, "Accurate Numerical Method for Calculating Frequency-Distribution Functions in Solids," *Physical Review* 144 (1966): 390–395.

46. W. E. Pickett and P. B. Allen, "Optical Properties of Nb and Mo Calculated from Augmented-Plane-Wave Band Structures," *Physical Review B* 11 (1975): 3599–3603

47. W. E. Pickett, TCM Group Report No. 8, TCM Group, Cavendish Laboratory, Cambridge, U.K. 1974 (unpublished). The linear tetrahedron integration method of Gilat and Raubenheimer [45] was extended to evaluate the integral of the double δ-function expression $\delta(\varepsilon_k)\delta(\varepsilon_{k+q})$ around the line of intersection of the Fermi surface and a Fermi surface displaced by q.

48. J. Kunstmann, "Density Functional and Linear Response Studies of *sp* Materials," PhD thesis, Max Planck Institute, Stuttgart, 2008 (unpublished).

49. C. R. Leavens and J. P. Carbotte, "An Important Parameter in High-Temperature Superconductivity," *Journal of Low Temperature Physics* 14 (1974): 195–211.

50. C. R. Leavens, "Important Parameters in Strong-coupling Superconductivity," *Journal of Physics F* 7 (1977): 1911–1922.

51. P. Giannozzi, O. Andreussi, T. Brumme, et al., "Advanced Capabilities for Materials Modeling with Quantum Espresso," *Journal of Physics: Condensed Matter* 29 (2017): 465901.

52. K. Dolui, L. J. Conway, C. Heil, T. A. Strobel, R. P. Prasankumar, and C. J. Pickard, "Feasible Route to High-Temperature Ambient-Pressure Hydride Superconductivity," *Physical Review Letters* 132 (2024): 166001.

53. G. Bergmann and D. Rainer, "The Sensitivity of the Transition Temperature to Changes in $\alpha^2F(\omega)$," *Zeitschrift für Physik* 263 (1973): 59–68.

54. J. A. Camargo-Martínez, G. I. González-Pedreros, and F. Mesa, "The Higher Superconducting Transition Temperature T_c and the Functional Derivative of T_c with $\alpha^2F(\omega)$ for Electron-Phonon Superconductors," *Journal of Physics: Condensed Matter* 32 (2020): 505901.

55. F. S. Khan and P. B. Allen, "Deformation Potentials and Electron-Phonon Scattering: Two New Theorems," *Physical Review* 29 (1984): 3341–3349.

56. W. Pickett and M. Eremets, "The Quest for Room-Temperature Superconductivity in Hydrides," *Physics Today* 72 (2019): 52–58. https://doi.org/10.1063/PT.3.4204.

57. S. Y. Savrasov, "Linear-Response Theory and Lattice Dynamics: A Muffin-Tin-Orbital Approach," *Physical Review B* 54 (1996): 16470–16486.

58. S. Y. Savrasov and D. Y. Savrasov, "Electron-Phonon Interactions and Related Physical Properties of Metals from Linear-Response Theory," *Physical Review B* 54 (1996): 16487–16501.

Appendix A: Example from Lithium Under Pressure

A.1 | The Enatom Deformation Potential

While the enatom picture has not yet been implemented in electron-phonon codes, there is one instructive example. Lithium, whose T_c increases around five decades of temperature from ambient to 35 GPa (sub-mK to 20K), was discussed in the text and referenced. Using finite difference calculations the enatom density and potential were straightforward to obtain [32, 48].

Figure A1 provides insight into the behavior of the potential deformation quantities (as labeled) of Li under displacement, *p* and *d* electron materials will display more complex behavior. The calculation was done in a $(3a)^3$ 108 atom fcc supercell (using the structure at the volume of the experimental pressure). The four panels picture the deformation density and potential character, and are described in the caption. A separate interesting result (not shown) is that the enatom rigid density contains

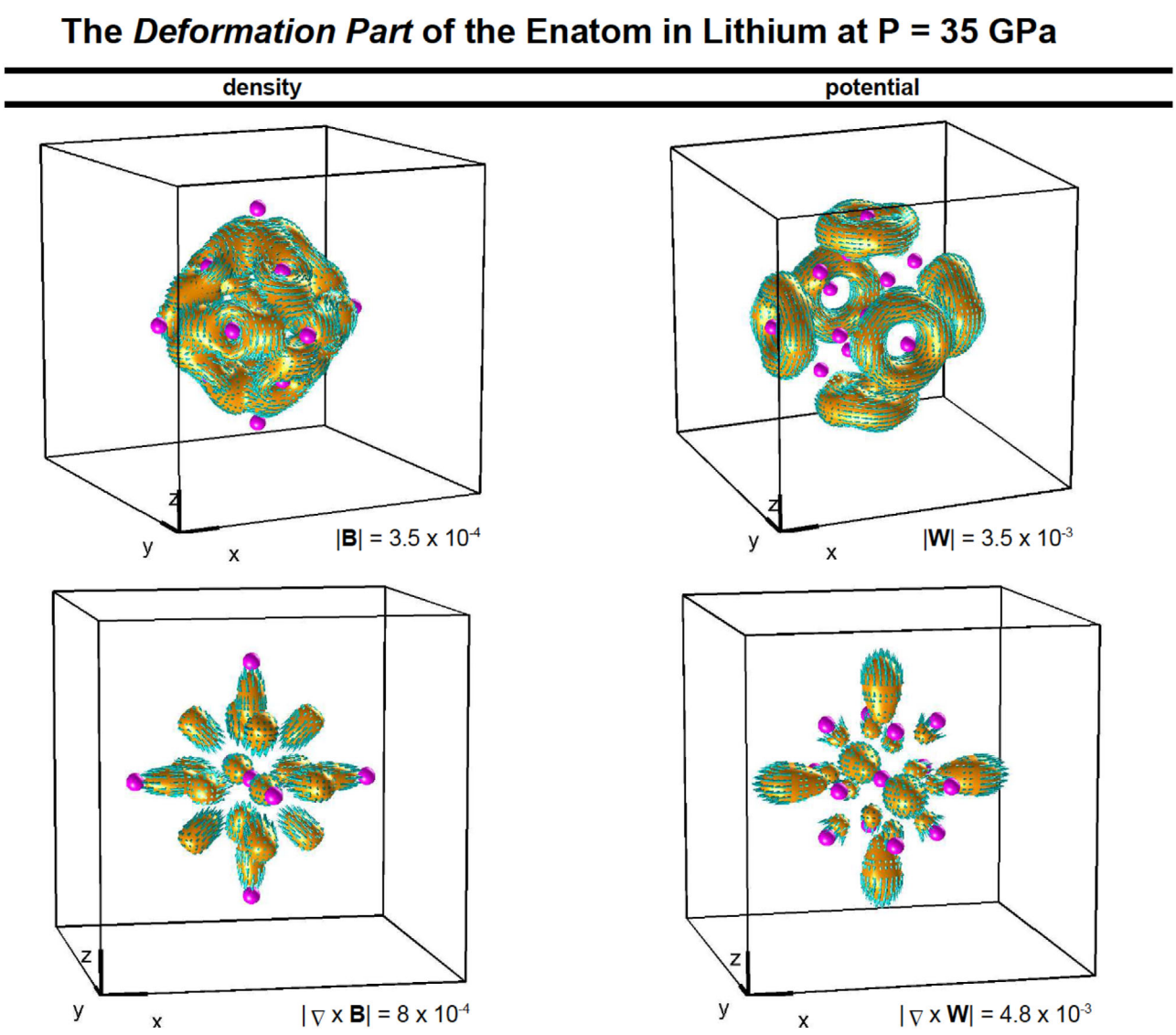

FIGURE A1 | Isosurface plots in a 3^3 supercell (108 atoms) of the enatom deformation density and deformation potential quantities for displacement of a Li atom:: gauge dependent $\vec{B}$ and $\vec{W}$, respectively (divergenceless gauge was chosen), and the physical quantities $\nabla \times \vec{B}$ and $\nabla \times \vec{W}$, respectively, for fcc lithium at 35 GPa. The directions of these vector quantities are denoted by arrows on the isosurfaces of their stated magnitude. $\vec{B}$ might be considered as a "beating heart" isosurface, with rather involved direction dependence on this surface but obeying the cubic symmetry of a cubic field. The deformation quantity $\vec{W}$ appears as swirling donuts near surrounding Li atoms in cubic symmetry form. Note that when the bottom two curl products are dotted into a displacement in the $+\hat{x}$ direction, the effect is to move density/potential from in front to behind the displaced atom – the deformation effect. These deformation effects appear to be small for Li, but no matrix elements have been calculated to allow assessment of their effect. The figure is adapted from the PhD thesis of J. Kunstmann [48] (unpublished).

a spherical shell of negative density somewhat beyond nearest neighbors with some angular variation, which would serve to make the lattice sum equal to the (positive) crystal density.

A.2 | Delicacy of Electron-Phonon Coupling

Figure A2 provides the values obtained for several parameters from calculations of 12^3 and 24^3 q-meshes, with k-meshes a factor of 2 finer in each of the three directions. These data reflect the large differences in α^2F that result for fcc Li at 35 GPa, even for fine k- and q-meshes never used for hydride superconductors. These differences are themselves the result of very small regions in the BZ with large nesting of the Fermi surfaces. As stated, even this fine mesh may not give the converged values of the various material properties. The calculations were done with Savrasov's linear muffin-tin orbital code [57, 58]. T_c was calculated from the Allen-Dynes equation [31].

The intricacy of the nesting function $\xi(q)$ in fcc Li is displayed in Figure A3. In spite of the very simple Fermi surface [43] the nesting function shows high intensity along narrow sheets through $\Gamma - X$ (near X) and around the K point of the zone. The phonon linewidth, i.e. the strength of electron-phonon coupling, is the nesting function with squared electron-phonon matrix elements inserted into the integrand. Matrix elements and other small q corrections will reduce the Γ point divergence of $\xi(q)$ to finite values of the coupling. Also, the small weight given to the Γ point (a single point in a 3D zone) in the integral usually does not leave much contribution to the net coupling, if the double δ-function is taken care of properly. The point is that even simple Fermi surfaces can have "hot spots" that make for slow convergence of integrals such as those for α^2F and λ. There are correspondingly sharp Kohn anomalies in the phonon spectrum that are lost with coarse meshes [43, 44]. The figure is reproduced from Ref. [43]. Copyright: American Physical Society.

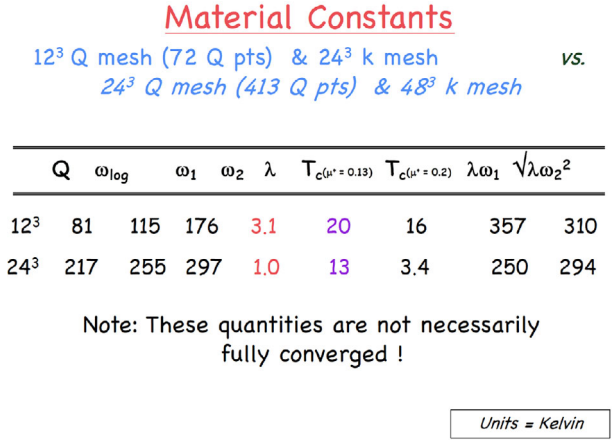

FIGURE A2 | A slide from a presentation of the calculation of Li superconductivity at 35 GPa [43, 44]. Even at quite fine k- and q-meshes on a very simple Fermi surface, halving the (already fine) mesh distance gives extremely different values of critical parameters, see λ and the frequency moments. The large uncertainties in λ and ω_{log} tend to offset in the resulting T_c, but leave confusion about what parameter(s) are important. The anomalies (large and sharply defined renormalization regions) occur [43, 44]. This figure (unpublished) is taken from a presentation by members of the author's research group [43, 44].

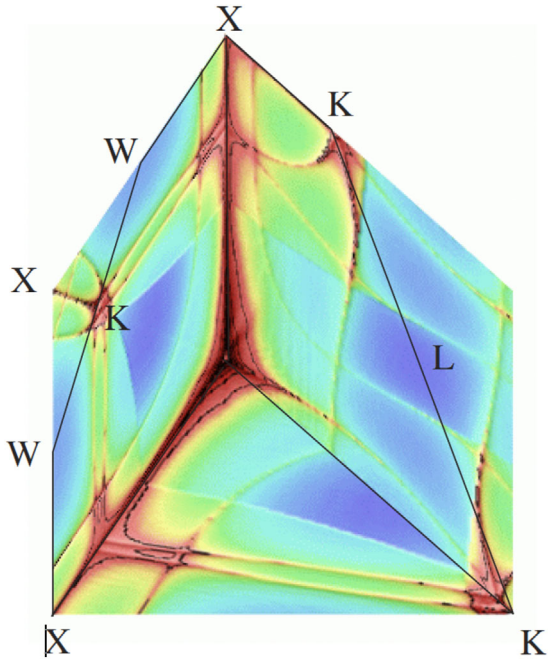

FIGURE A3 | A plot of the nesting function of fcc Li at 35 GPa where it is superconducting near 20 K, showing intensity plots throughout three of the high symmetry planes of the zone [43, 44]. Red indicates high intensity, deep blue is very low intensity. The deep red area at the center of the plot, at the Γ point, is a trivial and non-physical divergence of the nesting function. The narrow stripes and arcs of this nesting function are indicative of numerical difficulty in obtaining the volume integral, which relates (when matrix elements are included) to α^2F, coupling strength λ, phonon moments, and T_c. The figure is taken from Ref. [43]. Copyright: American Physical Society.